NANO LETTERS
Letter
Cite This: Nano Lett. 2018, 18, 5596−5602
pubs.acs.org/NanoLett

Two-Dimensional Band Structure in Honeycomb Metal−Organic Frameworks

Avijit Kumar,[†] Kaustuv Banerjee,[†] Adam S. Foster,[‡,¶,§] and Peter Liljeroth*[,†]

[†]Department of Applied Physics, Aalto University School of Science, PO Box 15100, 00076 Aalto, Finland
[‡]Department of Applied Physics, Aalto University School of Science, P.O. Box 11100, 00076 Aalto, Finland
[¶]WPI Nano Life Science Institute (WPI-NanoLSI), Kanazawa University, Kakuma-machi, Kanazawa 920-1192, Japan
[§]Graduate School Materials Science in Mainz, Staudinger Weg 9, 55128 Mainz, Germany

Supporting Information

ABSTRACT: Two-dimensional (2D) metal−organic frameworks (MOFs) have been recently proposed as a flexible material platform for realizing exotic quantum phases including topological and anomalous quantum Hall insulators. Experimentally, direct synthesis of 2D MOFs has been essentially confined to metal substrates, where the strong interaction with the substrate masks the intrinsic electronic properties of the MOF. In addition to electronic decoupling from the underlying metal support, synthesis on weakly interacting substrates (e.g., graphene) would enable direct realization of heterostructures of 2D MOFs with inorganic 2D materials. Here, we demonstrate synthesis of 2D honeycomb MOFs on epitaxial graphene substrate. Using low-temperature scanning tunneling microscopy (STM) and atomic force microscopy (AFM) complemented by density-functional theory (DFT) calculations, we show the formation of a 2D band structure in the MOF decoupled from the substrate. These results open the experimental path toward MOF-based designer electronic materials with complex, engineered electronic structures.

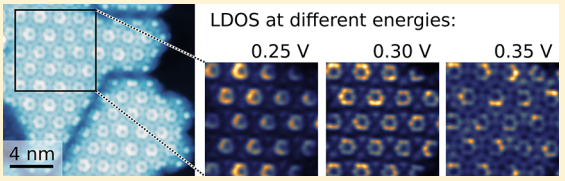

KEYWORDS: *Scanning tunneling microscopy (STM), metal−organic framework (MOF), cobalt, 4,4′-dicyanobiphenyl (DCBP), 9,10-dicyanoanthracene (DCA), epitaxial graphene*

Metal−organic frameworks (MOFs) are an important class of materials that present intriguing opportunities in the fields of sensing, gas storage, catalysis, and optoelectronics.[1−4] While there are a tremendous number of examples of three-dimensional, bulk MOFs, synthesis strategies for two-dimensional (2D), monolayer thick MOFs (also referred by various names[5] such as metal−organic coordination networks (MOCNs),[6] surface-confined metal−organic networks (SMONs),[7] metal−organic materials (MOMs), and metal−organic graphene analogues (MOGs)[8]) are more limited. These systems are drawing growing interest due to their very exciting properties, either in conjunction with other 2D materials or as a stand-alone platform for novel electronic materials with tunable properties.[9−11]

The synthetic flexibility and tunable electronic properties of MOFs stem from the choice of metal atoms, organic molecules, the linker chemistry and electronic and magnetic interactions among the building blocks.[7,12−16] For example, it is possible to realize honeycomb and Kagome lattices that are expected to give rise to peculiar electronic properties. Compared to 2D covalent organic framework (COFs), 2D MOFs can incorporate metal centers with high spin−orbit coupling and magnetism, which are important building blocks for realizing exotic materials such as topological and quantum anomalous Hall insulators. It has been theoretically predicted that 2D MOFs can be turned into topological insulators by adding sufficiently strong spin−orbit interactions through the choice of the metal atom.[13,14,17−19] This suggests MOFs as a tunable platform for realizing organic quantum materials.[9,13−20] Since 2D MOFs go through reversible bond-forming reactions, their on-surface synthesis on weakly interacting substrates is easier compared to 2D COFs.[21] However, experimental study of these materials requires synthesis methods that yield monolayer MOFs on weakly interacting substrates such that their intrinsic electronic properties can be probed.

Procedures for direct growth of 2D MOFs exist, e.g., through synthesis on the air−liquid interface or by chemical vapor deposition (CVD) in ultrahigh vacuum (UHV) conditions.[7,8,22−27] CVD growth is typically carried out on metallic substrates where various types of frameworks have been studied in detail.[7,12] However, the strong hybridization with the underlying substrate masks the intrinsic properties of the frameworks. This problem has been overcome in the case of single molecules by the use of ultrathin insulating films[28−31] and inert 2D materials such as graphene[10,32−35] that electronically decouple the molecule from the metallic substrate. Unfortunately, self-assembly and, in particular, on-surface

Received: May 21, 2018
Revised: August 8, 2018
Published: August 22, 2018

DOI: 10.1021/acs.nanolett.8b02062
Nano Lett. 2018, 18, 5596−5602

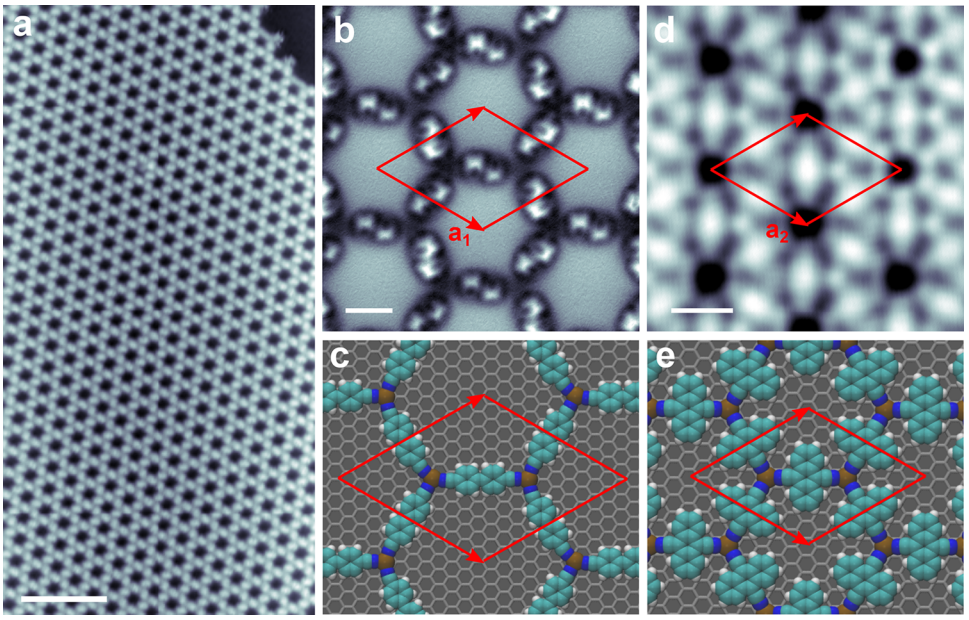

Figure 1. Overview of two MOFs. (a) An STM overview image of a honeycomb $DCBP_3Co_2$ MOF on G/Ir(111) surface. Scale bar is 10 nm. Imaging parameters: 1.23 V and 3.3 pA. (b) Constant height frequency-shift, Δf, nc-AFM image of $DCBP_3Co_2$ MOF acquired with a CO-terminated tip. Scale bar is 1 nm. (c) DFT-simulated structure of $DCBP_3Co_2$ MOF on graphene. (d) STM topography image of DCA_3Co_2 MOF. The scale bar is 1 nm. Imaging parameters: −1 V, 15 pA. (e) DFT simulated structure of DCA_3Co_2 MOF on graphene. Red parallelograms indicate the unit cells.

chemical reactions are a virtual *terra incognita* on weakly interacting, noncatalytic substrates[10,36−40] and therefore the experimental observation of the intrinsic electronic properties of 2D MOFs has been elusive. Here, we demonstrate the controlled synthesis of high quality honeycomb MOFs on epitaxial graphene using different organic linkers (dicyanobiphenyl, DCBP, and dicyanoanthracene, DCA) with cobalt metal atoms. We characterize the structures using low-temperature scanning tunneling microscopy (STM) and atomic force microscopy (AFM). We are able to access the intrinsic electronic properties of 2D MOFs and demonstrate the formation of a strongly coupled 2D electronic system in the DCA-Co MOF by scanning tunneling spectroscopy (STS) measurements complemented by density-functional theory (DFT) calculations.

Figure 1 shows the structure of the honeycomb MOFs—$DCBP_3Co_2$ and DCA_3Co_2—synthesized on epitaxial graphene grown on Ir(111) (G/Ir(111), experimental details are given in the Supporting Information). Briefly, after synthesis of epitaxial graphene,[41−43] we sequentially deposit the molecules and cobalt atoms at various temperatures. After deposition of a submonolayer coverage of the molecules, adding cobalt atoms at slightly elevated temperatures (details in the Supporting Information) results in formation of honeycomb MOFs. We did not observe any intercalation of Co at these annealing temperatures.[44] G/Ir(111) surface is the substrate of choice because of its weak geometric (∼50 pm) and work function (∼100 meV) corrugation across the moiré unit cell.[42,43,45]

Figure 1a shows an overview STM topography image of $DCBP_3Co_2$ MOF possessing a long-range ordered honeycomb structure. An atomically resolved non-contact AFM (nc-AFM) image of $DCBP_3Co_2$ MOF using a CO-terminated tip[46−48] is shown in Figure 1b. The hexagonal symmetry and nonplanarity of DCBP molecules (finite torsional angle between two phenyl rings along the long axis) making the framework chiral are readily apparent. This is consistent with the DFT calculated structure on graphene (Figure 1c) and simulated nc-AFM image as shown in the Supporting Information Figure S1. The calculated gas-phase structure shows that the cobalt atom is in the plane of the framework while it relaxes slightly (about 10 pm) toward the surface on graphene.

Similar to the $DCBP_3Co_2$, DCA_3Co_2 MOF also reveals a symmetric honeycomb structure as shown by the STM topography image in Figure 1d. A typical STM image of a large area DCA_3Co_2 MOF is shown in the Supporting Information, Figure S2, where various domains of different sizes are clearly visible. Compared to $DCBP_3Co_2$, the domains of the DCA_3Co_2 MOF are smaller in size probably due to the more limited mobility of DCA on the graphene surface. A DFT simulated structure corresponding to DCA_3Co_2 framework is shown in Figure 1e. Here also the DCA molecules and cobalt lie in the plane of the framework for gas-phase optimized structures (see Supporting Information for the computational details). In both MOFs, we estimate the N−Co coordination bond length from the high resolution STM images to be 1.5 ± 0.2 Å (see Supporting Information Figure S3) which is comparable to the value extracted from DFT relaxed structures and earlier reports.[23] Furthermore, the measured lattice constant of the $DCBP_3Co_2$ MOF, a_1 is 27.9 ± 0.4 Å while DCA_3Co_2 MOF possesses a lattice constant a_2 of 19.6 ± 0.2 Å (compared to the 27.3 and 20.0 Å as extracted from our DFT optimized structures, respectively).

We synthesize the MOFs by first depositing the organic molecules, followed by deposition of the metal atoms with subsequent annealing. Each of the honeycomb MOFs is separately preceded by the formation of an assembly of single complexes upon deposition of Co atoms on the molecular-layer on G/Ir(111) surface. The network of these complexes is stabilized through intermolecular hydrogen bonds between the cyano and phenyl groups. While DCBP forms 4-fold mononuclear single complexes ($DCBP_4Co$) and a stripe of 4-fold framework ($DCBP_3Co$) depending on the DCBP:Co

DOI: 10.1021/acs.nanolett.8b02062
Nano Lett. 2018, 18, 5596−5602

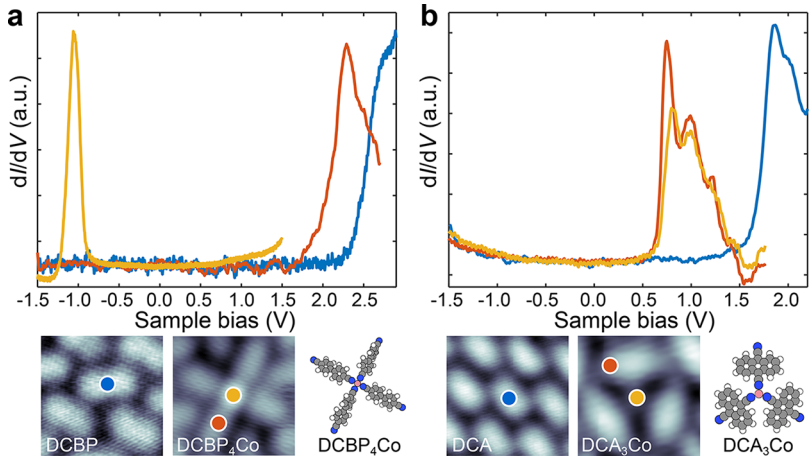

Figure 2. STS on single complexes. (a) dI/dV spectra measured on a single DCBP molecule (blue curve), and the Co atom (orange) and on the ligand (red) of a $DCBP_4Co$ complex. (b) dI/dV spectra measured on a single DCA molecule (blue curve), and the cobalt atoms (orange) and the ligand (red) on a single DCA_3Co complex. The positions of the spectra are shown on the bottom panels.

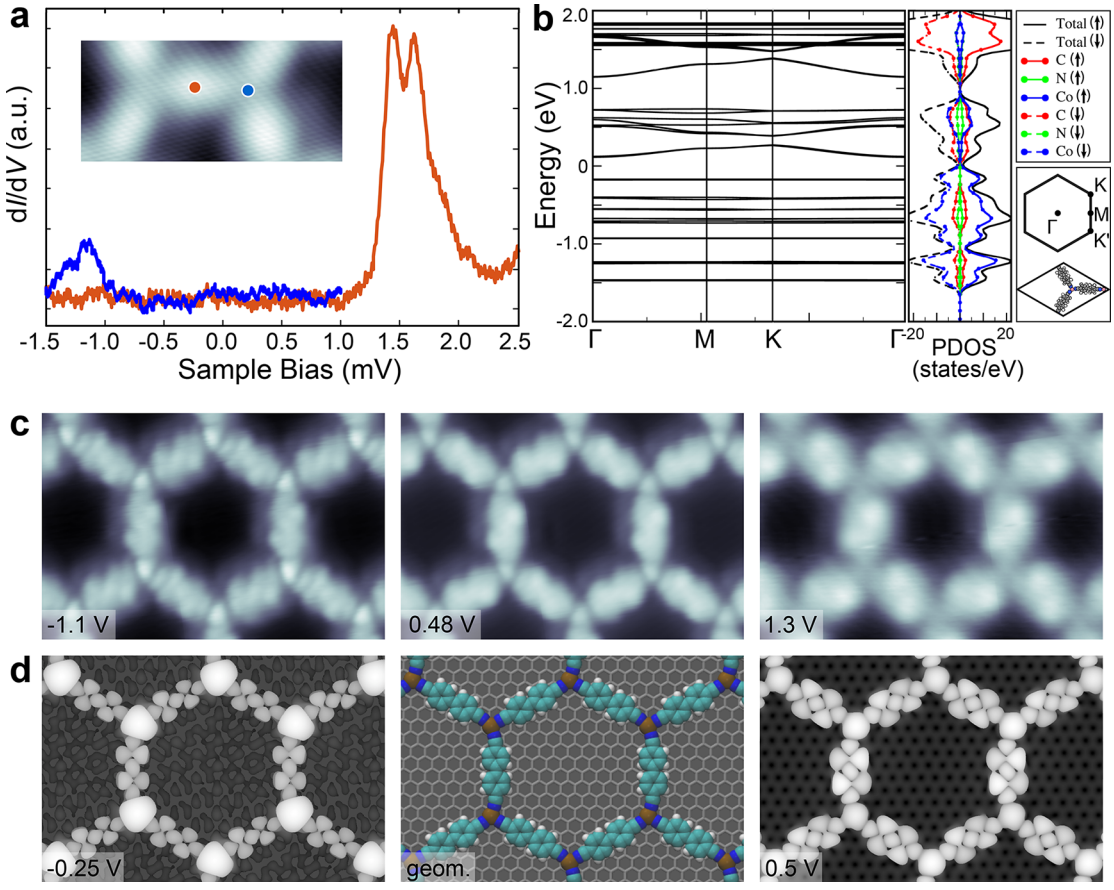

Figure 3. Electronic properties of honeycomb $DCBP_3Co_2$ MOF. (a) STS recorded on honeycomb $DCBP_3Co_2$ at the positions shown in the inset. (b) Calculated band structure and total PDOS of $DCBP_3Co_2$ MOF. (c, d) Experimental (panel c) and simulated STM images (panel d) at the energies indicated in the figure. Scan size is 6.2 × 4 nm^2.

stoichiometry, DCA forms only mononuclear 3-fold (DCA_3Co) complexes which is unambiguously confirmed by nc-AFM imaging (see Supporting Information, Figures S4 and S5). We attribute the absence of 4-fold DCA_4Co to a larger steric hindrance compared to that of a 4-fold structure of $DCBP_4Co$.

Figure 2 compares dI/dV spectra recorded on single molecules and the corresponding single metal−organic complexes. As shown in Figure 2a, dI/dV spectrum recorded on a DCBP molecule shows a shoulder at 2.7 V corresponding to the lowest unoccupied molecular orbital (LUMO) (see Supporting Information, Figure S5). The peak due to the highest occupied molecular orbital (HOMO) of the molecule is not accessible within the recorded bias range of the spectrum and it lies at a bias lower than −1.5 V. On a single $DCBP_4Co$ complex, dI/dV reveals two peaks at 2.3 V and −1 V with

DOI: 10.1021/acs.nanolett.8b02062
Nano Lett. 2018, 18, 5596−5602

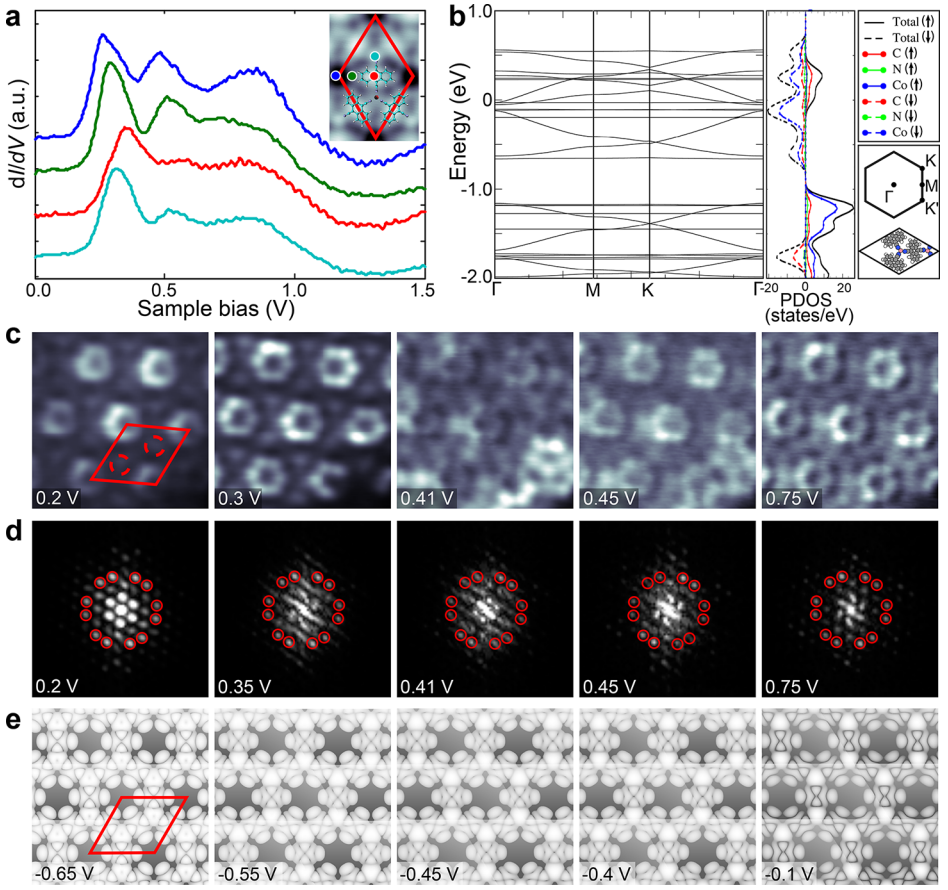

Figure 4. Electronic properties of honeycomb DCA_3Co_2 MOF. (a) STS recorded on honeycomb DCA_3Co_2 MOF on the positions indicated in the inset. (b) Calculated band structure and total PDOS of DCA_3Co_2 MOF. (c–e) Experimentally recorded constant-height dI/dV (panel c scan size 4.7 × 4.7 nm), FFTs of large area dI/dV maps (panel d), and simulated LDOS (panel e) at the energies indicated in the panels. The unit cell is indicated by the red parallelogram in panels c and e while the broken circles indicate the location of metal centers in panel c.

corresponding electronic states located on DCBP and Co center, respectively. On the basis of the bias-dependent STM imaging of the 4-fold phases and dI/dV spectroscopy of DCBP molecule as a function of distance from Co center (see Supporting Information, Figures S5 and S6), it is clear that the peak 2.3 V originates from the LUMO of the DCBP molecule. The shift of the molecular LUMO toward the Fermi level by 0.4 V indicates that there is an electrostatic shift of the orbital energy due to the Co atom of the complex and other complexes present in the vicinity.

dI/dV spectra on single DCA molecule on G/Ir(111) also reveal a peak at 1.8 V as shown in Figure 2b. The gating effect due to Co atoms is also observed in the DCA_3Co single complexes. The dI/dV spectra recorded on DCA of the complex shows that the LUMO shifts down to 750 mV and three satellite vibronic peaks also become visible. The vibronic mode energy of ∼200 mV fits well with the expected energy of the C−C vibration.[49,50] The assignment of the peak to the molecular LUMO is also evident from the STM images (see Supporting Information Figures S4 and S7). If there was (integer) charge transfer to DCBP or DCA molecules in the respective complexes, the LUMO peak would split to singly occupied/unoccupied molecular orbital (SOMO/SUMO) peaks at negative and positive bias.[51,52] dI/dV spectra recorded on Co center of the complex shows an additional shoulder at the onset of the peak. We attribute this shoulder to the metal-state as the metal center becomes brighter in the STM images at sample bias beyond 0.7 V (see Supporting Information Figure S4).

Figure 3a shows dI/dV spectra recorded on DCBP molecule in the $DCBP_3Co_2$ MOF has a peak at 1.44 V which we ascribe to the elastic LUMO peak with corresponding vibronic replica at 1.62 V. The small line-width of DCBP LUMO and the observation of satellite vibronic peaks indicate that the intermolecular electronic coupling in the framework is weak such that we have isolated molecular electronic states. The spectrum recorded on the Co center reveals a faint peak at −1150 mV, which is visible in the background corrected spectrum (see Supporting Information Figure S8). The state is localized only at the metal-center.

We have used DFT to calculate the band structure of the $DCBP_3Co_2$ MOF as shown in Figure 3b for the antiferromagnetic ground state. While DFT underestimates the band gap, it correctly captures the nature of the lowest lying bands: the occupied states have a stronger metal character compared to the unoccupied states, which are mostly composed of the ligand states (Figure 3c,d). The enhanced contrast on the metal atoms and ligands can be seen at negative and positive bias, respectively, compared to the STM topography in the gap (Figure 3c, middle panel). However, DFT seems to overestimate the bandwidth of the unoccupied ligand-derived states compared to the experiment. This could be related to how well the torsional angle between the phenyl rings of DCBP molecule is estimated by DFT as this is known to control

DOI: 10.1021/acs.nanolett.8b02062
Nano Lett. 2018, 18, 5596−5602

the $\pi-\pi$ conjugation within the backbone of the molecule.[53] The coupling is enhanced for the planar, smaller DCA linker as demonstrated below.

A substantial in-plane electronic hybridization and formation of energy bands with significant width in DCA_3Co_2 MOF is evidenced by dI/dV spectroscopy and spatially resolved dI/dV maps. dI/dV spectrum (Figure 4, blue) recorded at the center of the ring (constituting six DCA lobes) has three peaks at 260, 480, and 860 mV. Considering the separation between the first and the second peak, ~ 220 mV, the second peak could still be interpreted as a vibronic satellite. However, the separation between the second and the third peak rules out vibronic origin. The spectrum at the center of DCA molecule (red curve) shows that the first peak shifts to 360 mV, while that on cobalt (cyan curve) has the first peak at 320 mV. The systematic evolution of the spectra across the framework is shown in the Supporting Information Figure S9. Comparison of the spectra at the lobe and center of DCA and cobalt in the DCA_3Co_2 MOF to that of DCA_3Co single complex indicates that there is additional intensity in the MOF at energies higher than 700 mV (see Supporting Information Figure S10). As the dI/dV signal is directly proportional to the local density of states (LDOS), this is direct evidence of additional electronic states. Further, we have recorded dI/dV maps of the same area at different energies as shown in Figure 4c. The LUMO lobes on the DCA molecules are the brightest feature at lowest energies (200 mV), while the states on the Co sites are more prominent at ~300 mV. At intermediate energies, 410 and 450 mV, there exist extra bright features in the dI/dV maps superimposed on the existing framework. These features are likely to result from the formation of standing wave patterns due to the scattering of 2D electron waves from the boundaries of the finite sized DCA_3Co_2 MOF domain. This is supported by the Fourier transforms (FFT) of a large area dI/dV maps (Figure 4d). Apart from the 12 outer spots (red circles) corresponding to the honeycomb structure of DCA_3Co_2 MOF, there exists internal structure which evolves continuously with the bias. The spots in this quasi-particle interference pattern correspond to scattering vectors connecting the initial and final states of the scattering process at the given energy. In addition to this joint density-of-states, they contain information on the nature of the allowed scattering processes.[54−56] While quantitative analysis of the experimental patterns is difficult due to the other overlapping peaks stemming from the geometry as well as the limited sample size (number of repetitive unit cells), they indicate the formation of an extended electron system with considerable dispersion (bandwidth).

The calculated electronic band structure using DFT for the symmetric, ferromagnetic DCA_3Co_2 framework without graphene is shown in Figure 4b. The band structure on graphene has additional bands arising from the graphene and the slight shifts and splittings of the MOF states are due to the residual interaction with the graphene (see Supporting Information, Figure S11). In line with the calculations done for DCA_3Cu_2 and DCA_3Mn_2 MOFs,[18,20] the band structure of DCA_3Co_2 MOF has a number of flat-bands and Dirac cones. While the antiferromagnetic structure is slightly lower in energy (by 0.05 eV), the ferromagnetic state better reproduces the experimental results (see also discussion on this in the computational methods section of the Supporting Information). LDOS maps of DCA_3Co_2 MOF for both spin configurations look very similar except for the map at −0.15 V corresponding to antiferromagnetic configuration (see Supporting Information, Figure S12b), where prominent metal states stand out. These are not observed experimentally, suggesting a ferromagnetic spin configuration. The presence of a large gap between −0.7 and −1.2 eV in the calculated band structure and lack of states below the Fermi energy in the dI/dV spectra until −1.5 V suggest that the energy corresponding to the experimental Fermi level lies below the flat band at energy −0.7 V. The DFT calculation suggests that the bottom of the conduction band consists of a flat band and a Dirac cone stemming from the DCA states and the Kagome symmetry of the lattice. Subsequently, at higher energies, there are also relatively flat bands originating mostly from the metal atom orbitals and a band with more mixed character. This overall picture is consistent with the experiments where we first see intensity on the molecules with metal states emerging at higher energies and an overall bandwidth of ~1 eV.

In summary, we have demonstrated direct synthesis of high-quality honeycomb MOFs on epitaxial graphene surface. While $DCBP_3Co_2$ MOF only has weak coupling between the building blocks, DCA_3Co_2 MOF shows significant in-plane hybridization resulting in the formation of 2D electronic states with significant bandwidth. These results open the experimental path toward MOF-based designer electronic materials with complex, engineered electronic structures. The direct growth of 2D MOFs on graphene outlines possibilities of heterostructures with inorganic 2D materials with potential applications in electronics, sensors, and catalysis.

■ ASSOCIATED CONTENT

Supporting Information

The Supporting Information is available free of charge on the ACS Publications website at DOI: 10.1021/acs.nanolett.8b02062.

Experimental and computational methods and additional results (PDF)

■ AUTHOR INFORMATION

Corresponding Author

*(P.L.) E-mail: peter.liljeroth@aalto.fi.

ORCID

Adam S. Foster: 0000-0001-5371-5905

Peter Liljeroth: 0000-0003-1253-8097

Notes

The authors declare no competing financial interest.

■ ACKNOWLEDGMENTS

This research made use of the Aalto Nanomicroscopy Center (Aalto NMC) facilities and was supported by the European Research Council (ERC-2017-AdG No. 788185 "Artificial Designer Materials"), and the Academy of Finland (Projects no. 305635 and 311012, and Centres of Excellence Program projects no. 284594 and 284621). A.S.F. has been supported by the World Premier International Research Center Initiative (WPI), MEXT, Japan and acknowledges use of the CSC, Helsinki for computational resources.

■ REFERENCES

(1) Hendon, C. H.; Rieth, A. J.; Korzyński, M. D.; Dincă, M. Grand Challenges and Future Opportunities for Metal-Organic Frameworks. *ACS Cent. Sci.* **2017**, *3*, 554−563.

DOI: 10.1021/acs.nanolett.8b02062
Nano Lett. 2018, 18, 5596−5602

(2) Kreno, L. E.; Leong, K.; Farha, O. K.; Allendorf, M.; Van Duyne, R. P.; Hupp, J. T. Metal-Organic Framework Materials as Chemical Sensors. *Chem. Rev.* **2012**, *112*, 1105−1125.
(3) Zhu, L.; Liu, X.-Q.; Jiang, H.-L.; Sun, L.-B. Metal-Organic Frameworks for Heterogeneous Basic Catalysis. *Chem. Rev.* **2017**, *117*, 8129−8176.
(4) Stavila, V.; Talin, A. A.; Allendorf, M. D. MOF-Based Electronic and Opto-Electronic Devices. *Chem. Soc. Rev.* **2014**, *43*, 5994−6010.
(5) Seth, S.; Matzger, A. J. Metal-Organic Frameworks: Examples, Counterexamples, and an Actionable Definition. *Cryst. Growth Des.* **2017**, *17*, 4043−4048.
(6) Stepanow, S.; Lingenfelder, M.; Dmitriev, A.; Spillmann, H.; Delvigne, E.; Lin, N.; Deng, X.; Cai, C.; Barth, J. V.; Kern, K. Steering Molecular Organization and Host-Guest Interactions Using Two-Dimensional Nanoporous Coordination Systems. *Nat. Mater.* **2004**, *3*, 229.
(7) Dong, L.; Gao, Z. A.; Lin, N. Self-assembly of metal-organic coordination structures on surfaces. *Prog. Surf. Sci.* **2016**, *91*, 101−135.
(8) Sheberla, D.; Sun, L.; Blood-Forsythe, M. A.; Er, S.; Wade, C. R.; Brozek, C. K.; Aspuru-Guzik, A.; Dinca, M. High Electrical Conductivity in Ni_3(2,3,6,7,10,11-hexaiminotriphenylene)$_2$, a Semiconducting Metal-Organic Graphene Analogue. *J. Am. Chem. Soc.* **2014**, *136*, 8859−8862.
(9) Basov, D. N.; Averitt, R. D.; Hsieh, D. Towards properties on demand in quantum materials. *Nat. Mater.* **2017**, *16*, 1077.
(10) Kumar, A.; Banerjee, K.; Liljeroth, P. Molecular Assembly on Two-Dimensional Materials. *Nanotechnology* **2017**, *28*, 082001.
(11) Jakobs, S.; Narayan, A.; Stadtmüller, B.; Droghetti, A.; Rungger, I.; Hor, Y. S.; Klyatskaya, S.; Jungkenn, D.; Stöckl, J.; Laux, M.; Monti, O. L. A.; Aeschlimann, M.; Cava, R. J.; Ruben, M.; Mathias, S.; Sanvito, S.; Cinchetti, M. Controlling the Spin Texture of Topological Insulators by Rational Design of Organic Molecules. *Nano Lett.* **2015**, *15*, 6022−6029.
(12) Barth, J. V. Molecular Architectonic on Metal Surfaces. *Annu. Rev. Phys. Chem.* **2007**, *58*, 375−407.
(13) Wang, Z. F.; Su, N.; Liu, F. Prediction of a Two-Dimensional Organic Topological Insulator. *Nano Lett.* **2013**, *13*, 2842−2845.
(14) Dong, L.; Kim, Y.; Er, D.; Rappe, A. M.; Shenoy, V. B. Two-Dimensional π-Conjugated Covalent-Organic Frameworks as Quantum Anomalous Hall Topological Insulators. *Phys. Rev. Lett.* **2016**, *116*, 096601.
(15) Zhang, X.; Zhou, Y.; Cui, B.; Zhao, M.; Liu, F. Theoretical Discovery of a Superconducting Two-Dimensional Metal-Organic Framework. *Nano Lett.* **2017**, *17*, 6166−6170.
(16) Yamada, M. G.; Dwivedi, V.; Hermanns, M. Crystalline Kitaev spin liquids. *Phys. Rev. B: Condens. Matter Mater. Phys.* **2017**, *96*, 155107.
(17) Wang, Z. F.; Liu, Z.; Liu, F. Organic Topological Insulators in Organometallic Lattices. *Nat. Commun.* **2013**, *4*, 1471.
(18) Zhang, L. Z.; Wang, Z. F.; Huang, B.; Cui, B.; Wang, Z.; Du, S. X.; Gao, H.-J.; Liu, F. Intrinsic Two-Dimensional Organic Topological Insulators in Metal-Dicyanoanthracene Lattices. *Nano Lett.* **2016**, *16*, 2072−2075.
(19) Sun, H.; Tan, S.; Feng, M.; Zhao, J.; Petek, H. Deconstruction of the Electronic Properties of a Topological Insulator with a Two-Dimensional Noble Metal-Organic Honeycomb-Kagome Band Structure. *J. Phys. Chem. C* **2018**, *122*, 18659.
(20) Wang, Y.-P.; Ji, W.-X.; Zhang, C.-W.; Li, P.; Wang, P.-J.; Kong, B.; Li, S.-S.; Yan, S.-S.; Liang, K. Discovery of intrinsic quantum anomalous Hall effect in organic Mn-DCA lattice. *Appl. Phys. Lett.* **2017**, *110*, 233107.
(21) Diercks, C. S.; Yaghi, O. M. The atom, the molecule, and the covalent organic framework. *Science* **2017**, *355*, eaal1585.
(22) Kambe, T.; Sakamoto, R.; Hoshiko, K.; Takada, K.; Miyachi, M.; Ryu, J.-H.; Sasaki, S.; Kim, J.; Nakazato, K.; Takata, M.; Nishihara, H. π-Conjugated Nickel Bis(dithiolene) Complex Nanosheet. *J. Am. Chem. Soc.* **2013**, *135*, 2462−2465.
(23) Schlickum, U.; Decker, R.; Klappenberger, F.; Zoppellaro, G.; Klyatskaya, S.; Ruben, M.; Silanes, I.; Arnau, A.; Kern, K.; Brune, H.; Barth, J. V. Metal-Organic Honeycomb Nanomeshes with Tunable Cavity Size. *Nano Lett.* **2007**, *7*, 3813−3817.
(24) Pawin, G.; Wong, K. L.; Kim, D.; Sun, D.; Bartels, L.; Hong, S.; Rahman, T. S.; Carp, R.; Marsella, M. A Surface Coordination Network Based on Substrate-Derived Metal Adatoms with Local Charge Excess. *Angew. Chem., Int. Ed.* **2008**, *47*, 8442−8445.
(25) Stepanow, S.; Lin, N.; Payer, D.; Schlickum, U.; Klappenberger, F.; Zoppellaro, G.; Ruben, M.; Brune, H.; Barth, J.; Kern, K. Surface-Assisted Assembly of 2D Metal-Organic Networks That Exhibit Unusual Threefold Coordination Symmetry. *Angew. Chem., Int. Ed.* **2007**, *46*, 710−713.
(26) Clough, A. J.; Yoo, J. W.; Mecklenburg, M. H.; Marinescu, S. C. Two-Dimensional Metal-Organic Surfaces for Efficient Hydrogen Evolution from Water. *J. Am. Chem. Soc.* **2015**, *137*, 118−121.
(27) Sakamoto, R.; Takada, K.; Pal, T.; Maeda, H.; Kambe, T.; Nishihara, H. Coordination Nanosheets (CONASHs): Strategies, Structures and Functions. *Chem. Commun.* **2017**, *53*, 5781−5801.
(28) Qiu, X. H.; Nazin, G. V.; Ho, W. Vibrationally Resolved Fluorescence Excited with Submolecular Precision. *Science* **2003**, *299*, 542−546.
(29) Repp, J.; Meyer, G.; Stojković, S. M.; Gourdon, A.; Joachim, C. Molecules on Insulating Films: Scanning-Tunneling Microscopy Imaging of Individual Molecular Orbitals. *Phys. Rev. Lett.* **2005**, *94*, 026803.
(30) Swart, I.; Gross, L.; Liljeroth, P. Single-molecule chemistry and physics explored by low-temperature scanning probe microscopy. *Chem. Commun.* **2011**, *47*, 9011−9023.
(31) Schulz, F.; Ijäs, M.; Drost, R.; Hämäläinen, S. K.; Harju, A.; Seitsonen, A. P.; Liljeroth, P. Many-body transitions in a single molecule visualized by scanning tunnelling microscopy. *Nat. Phys.* **2015**, *11*, 229−234.
(32) Järvinen, P.; Hämäläinen, S. K.; Banerjee, K.; Häkkinen, P.; Ijäs, M.; Harju, A.; Liljeroth, P. Molecular Self-Assembly on Graphene on SiO_2 and h-BN Substrates. *Nano Lett.* **2013**, *13*, 3199−3204.
(33) Järvinen, P.; Hämäläinen, S. K.; Ijäs, M.; Harju, A.; Liljeroth, P. Self-Assembly and Orbital Imaging of Metal Phthalocyanines on a Graphene Model Surface. *J. Phys. Chem. C* **2014**, *118*, 13320−13325.
(34) Riss, A.; Wickenburg, S.; Tan, L. Z.; Tsai, H.-Z.; Kim, Y.; Lu, J.; Bradley, A. J.; Ugeda, M. M.; Meaker, K. L.; Watanabe, K.; Taniguchi, T.; Zettl, A.; Fischer, F. R.; Louie, S. G.; Crommie, M. F. Imaging and Tuning Molecular Levels at the Surface of a Gated Graphene Device. *ACS Nano* **2014**, *8*, 5395−5401.
(35) Banerjee, K.; Kumar, A.; Canova, F. F.; Kezilebieke, S.; Foster, A. S.; Liljeroth, P. Flexible Self-Assembled Molecular Templates on Graphene. *J. Phys. Chem. C* **2016**, *120*, 8772−8780.
(36) Abel, M.; Clair, S.; Ourdjini, O.; Mossoyan, M.; Porte, L. Single Layer of Polymeric Fe-Phthalocyanine: An Organometallic Sheet on Metal and Thin Insulating Film. *J. Am. Chem. Soc.* **2011**, *133*, 1203−1205.
(37) Dienel, T.; Gómez-Díaz, J.; Seitsonen, A. P.; Widmer, R.; Iannuzzi, M.; Radican, K.; Sachdev, H.; Müllen, K.; Hutter, J.; Gröning, O. Dehalogenation and Coupling of a Polycyclic Hydrocarbon on an Atomically Thin Insulator. *ACS Nano* **2014**, *8*, 6571−6579.
(38) Morchutt, C.; Björk, J.; Krotzky, S.; Gutzler, R.; Kern, K. Covalent Coupling via Dehalogenation on Ni(111) Supported Boron Nitride and Graphene. *Chem. Commun.* **2015**, *51*, 2440−2443.
(39) Guo, C.; Wang, Y.; Kittelmann, M.; Kantorovitch, L.; Kühnle, A.; Floris, A. Mechanisms of Covalent Dimerization on a Bulk Insulating Surface. *J. Phys. Chem. C* **2017**, *121*, 10053−10062.
(40) Schüller, L.; Haapasilta, V.; Kuhn, S.; Pinto, H.; Bechstein, R.; Foster, A. S.; Kühnle, A. Deposition Order Controls the First Stages of a Metal-Organic Coordination Network on an Insulator Surface. *J. Phys. Chem. C* **2016**, *120*, 14730−14735.
(41) N'Diaye, A. T.; Coraux, J.; Plasa, T. N.; Busse, C.; Michely, T. Structure of Epitaxial Graphene on Ir(111). *New J. Phys.* **2008**, *10*, 043033.

DOI: 10.1021/acs.nanolett.8b02062
Nano Lett. 2018, 18, 5596−5602

(42) Busse, C.; Lazić, P.; Djemour, R.; Coraux, J.; Gerber, T.; Atodiresei, N.; Caciuc, V.; Brako, R.; N'Diaye, A. T.; Blügel, S.; Zegenhagen, J.; Michely, T. Graphene on Ir(111): Physisorption with Chemical Modulation. *Phys. Rev. Lett.* **2011**, *107*, 036101.
(43) Hämäläinen, S. K.; Boneschanscher, M. P.; Jacobse, P. H.; Swart, I.; Pussi, K.; Moritz, W.; Lahtinen, J.; Liljeroth, P.; Sainio, J. Structure and Local Variations of the Graphene Moiré on Ir(111). *Phys. Rev. B: Condens. Matter Mater. Phys.* **2013**, *88*, 201406.
(44) Decker, R.; Brede, J.; Atodiresei, N.; Caciuc, V.; Blügel, S.; Wiesendanger, R. Atomic-scale magnetism of cobalt-intercalated graphene. *Phys. Rev. B: Condens. Matter Mater. Phys.* **2013**, *87*, 041403.
(45) Altenburg, S. J.; Berndt, R. Local Work Function and STM Tip-Induced Distortion of Graphene on Ir(111). *New J. Phys.* **2014**, *16*, 053036.
(46) Gross, L.; Mohn, F.; Moll, N.; Liljeroth, P.; Meyer, G. The Chemical Structure of a Molecule Resolved by Atomic Force Microscopy. *Science* **2009**, *325*, 1110−1114.
(47) Schulz, F.; Hämäläinen, S.; Liljeroth, P. Atomic-Scale Contrast Formation in AFM Images on Molecular Systems. *Noncontact Atomic Force Microscopy* **2015**, *3*, 173−194.
(48) Pavliček, N.; Gross, L. Generation, Manipulation and Characterization of Molecules by Atomic Force Microscopy. *Nat. Rev. Chem.* **2017**, *1*, 0005.
(49) Repp, J.; Liljeroth, P.; Meyer, G. Coherent Electron-Nuclear Coupling in Oligothiophene Molecular Wires. *Nat. Phys.* **2010**, *6*, 975−979.
(50) van der Lit, J.; Boneschanscher, M. P.; Vanmaekelbergh, D.; Ijäs, M.; Uppstu, A.; Ervasti, M.; Harju, A.; Liljeroth, P.; Swart, I. Suppression of Electron-Vibron Coupling in Graphene Nanoribbons Contacted via a Single Atom. *Nat. Commun.* **2013**, *4*, 2023.
(51) Repp, J.; Meyer, G.; Paavilainen, S.; Olsson, F. E.; Persson, M. Imaging Bond Formation Between a Gold Atom and Pentacene on an Insulating Surface. *Science* **2006**, *312*, 1196−1199.
(52) Kumar, A.; Banerjee, K.; Dvorak, M.; Schulz, F.; Harju, A.; Rinke, P.; Liljeroth, P. Charge-Transfer-Driven Nonplanar Adsorption of F_4TCNQ Molecules on Epitaxial Graphene. *ACS Nano* **2017**, *11*, 4960−4968.
(53) Venkataraman, L.; Klare, J. E.; Nuckolls, C.; Hybertsen, M. S.; Steigerwald, M. L. Dependence of Single-Molecule Junction Conductance on Molecular Conformation. *Nature* **2006**, *442*, 904−907.
(54) Petersen, L.; Hofmann, P.; Plummer, E. W.; Besenbacher, F. Fourier Transform-STM: Determining the Surface Fermi Contour. *J. Electron Spectrosc. Relat. Phenom.* **2000**, *109*, 97−115.
(55) Hoffman, J. E.; Hudson, E. W.; Lang, K. M.; Madhavan, V.; Eisaki, H.; Uchida, S.; Davis, J. C. A Four Unit Cell Periodic Pattern of Quasi-Particle States Surrounding Vortex Cores in $Bi_2Sr_2CaCu_2O_{8+\delta}$. *Science* **2002**, *295*, 466−469.
(56) Roushan, P.; Seo, J.; Parker, C. V.; Hor, Y. S.; Hsieh, D.; Qian, D.; Richardella, A.; Hasan, M. Z.; Cava, R. J.; Yazdani, A. Topological Surface States Protected from Backscattering by Chiral Spin Texture. *Nature* **2009**, *460*, 1106.

DOI: 10.1021/acs.nanolett.8b02062
Nano Lett. 2018, 18, 5596−5602